Neuro-Oncology

22(6), 819–829, 2020 | doi:10.1093/neuonc/noaa052 | Advance Access date 8 May 2020

Entrectinib, a TRK/ROS1 inhibitor with anti-CNS tumor activity: differentiation from other inhibitors in its class due to weak interaction with P-glycoprotein

Holger Fischer, Mohammed Ullah, Cecile C. de la Cruz, Thomas Hunsaker, Claudia Senn, Thomas Wirz, Björn Wagner, Dragomir Draganov, Faye Vazvaei, Massimiliano Donzelli, Axel Paehler, Mark Merchant, and Li Yu

Roche Pharma Research and Early Development, Pharmaceutical Sciences, Roche Innovation Centre Basel, Switzerland (H.F., M.U., C.S., T.W., B.W., D.D., M.D., A.P.); Genentech Research and Early Development, CA, USA (C.C.d.l.C., T.H., M.M.); Roche Pharma Research and Early Development, Pharmaceutical Sciences, Roche Translational and Clinical Research Center, Inc., NJ, USA (F.V., L.Y.)

Corresponding Author: Li Yu, Roche Pharma Research and Early Development, Roche Translational and Clinical Research Center, Inc. 150 Clove Road, 7th Floor, Little Falls, NJ 07424, USA (lijuliayu2@gmail.com).

Abstract

Background. Studies evaluating the CNS penetration of a novel tyrosine kinase inhibitor, entrectinib, proved challenging, particularly due to discrepancies across earlier experiments regarding P-glycoprotein (P-gp) interaction and brain distribution. To address this question, we used a novel "apical efflux ratio" (AP-ER) model to assess P-gp interaction with entrectinib, crizotinib, and larotrectinib, and compared their brain-penetration properties.

Methods. AP-ER was designed to calculate P-gp interaction with the 3 drugs in vitro using P-gp–overexpressing cells. Brain penetration was studied in rat plasma, brain, and cerebrospinal fluid (CSF) samples after intravenous drug infusion. Unbound brain concentrations were estimated through kinetic lipid membrane binding assays and ex vivo experiments, while the antitumor activity of entrectinib was evaluated in a clinically relevant setting using an intracranial tumor mouse model.

Results. Entrectinib showed lower AP-ER (1.1–1.15) than crizotinib and larotrectinib (≥2.8). Despite not reaching steady-state brain exposures in rats after 6 hours, entrectinib presented a more favorable CSF-to-unbound concentration in plasma ($CSF/C_{u,p}$) ratio (>0.2) than crizotinib and larotrectinib at steady state (both: $CSF/C_{u,p}$ ~0.03). In vivo experiments validated the AP-ER approach. Entrectinib treatment resulted in strong tumor inhibition and full survival benefit in the intracranial tumor model at clinically relevant systemic exposures.

Conclusions. Entrectinib, unlike crizotinib and larotrectinib, is a weak P-gp substrate that can sustain CNS exposure based on our novel in vitro and in vivo experiments. This is consistent with the observed preclinical and clinical efficacy of entrectinib in neurotrophic tropomyosin receptor kinase (*NTRK*) and *ROS1* fusion-positive CNS tumors and secondary CNS metastases.

Key Points

1. Entrectinib is a weak P-gp substrate with favorable brain distribution.
2. Crizotinib and larotrectinib are strong P-gp substrates with poor brain distribution.
3. Entrectinib showed strong anti-CNS tumor activity in vivo.

© The Author(s) 2020. Published by Oxford University Press on behalf of the Society for Neuro-Oncology.
This is an Open Access article distributed under the terms of the Creative Commons Attribution Non-Commercial License (http://creativecommons.org/licenses/by-nc/4.0/), which permits non-commercial re-use, distribution, and reproduction in any medium, provided the original work is properly cited. For commercial re-use, please contact journals.permissions@oup.com

Importance of the Study

Unmet needs exist for the treatment of CNS metastases expressing gene fusions of *ROS1* or *NTRK*; most anticancer drugs cannot achieve adequate exposure in the CNS mainly because they are substrates of P-gp, a key efflux transporter of the blood–brain barrier. Here, we used a novel approach to demonstrate that entrectinib, a potent inhibitor of tropomyosin-related kinase A/B/C and ROS1, is a weak substrate of P-gp and achieves therapeutic levels in the CNS, associated with strong efficacy in brain tumor models. Crizotinib and larotrectinib (inhibitors of the same class), on the contrary, are strong P-gp substrates with poor CNS exposure. These results can provide a scientific rationale to physicians when considering therapeutic options for patients with primary CNS tumors or CNS metastases harboring *ROS1* or *NTRK* fusions. Additionally, our findings have broad implications for the preclinical characterization of new molecular entities for treating CNS cancers.

Fusions involving tyrosine kinase genes such as *ROS1*, neurotrophic tropomyosin receptor kinase (*NTRK*), and anaplastic lymphoma kinase (*ALK*) result in the expression of constitutively active chimeric proteins. These proteins can act as oncogenic drivers across a broad range of tumor types, including extracranial solid tumors associated with high rates of metastasis to the CNS.[1] Up to 40% of patients with cancer develop brain metastases[2]; for example, incidences of brain metastases of up to 50% have been reported in patients with non-small-cell lung cancer (NSCLC).[3]

Developing effective treatments for CNS metastases in *ROS1* or *NTRK* fusion-positive cancers has been challenging, partially due to a lack of available CNS-penetrant anticancer agents. Many tyrosine kinase inhibitors (TKIs) are strong substrates of P-glycoprotein (P-gp), a key efflux transporter located at the blood–brain barrier that actively transports them out of the brain.[4,5] As a result, these TKIs have poor CNS efficacy, consistent with their limited capacity to sustain sufficient exposure in the brain.[6,7]

Crizotinib was the first-in-class treatment for *ROS1* and *ALK* fusion-positive NSCLC but it has not demonstrated intracranial efficacy in these settings, suggesting that the CNS exposure of this drug may be inadequate to control CNS disease.[8,9] Similarly, the US prescribing information for larotrectinib, the first tropomyosin-related kinase (TRK) inhibitor approved by the FDA, does not describe any intracranial efficacy,[10] and intracranial benefit following larotrectinib treatment has only been reported in a few patients with *NTRK* fusion-positive tumors and CNS involvement.[6,11] Importantly, crizotinib and larotrectinib are both known substrates for P-gp.[12,13]

Therefore, an unmet medical need exists for effective treatments with CNS activity for patients with *ROS1* fusion-positive NSCLC and *NTRK* fusion-positive tumors.

Entrectinib is a novel, potent, and orally bioavailable inhibitor of TRKA/B/C, ROS1, and ALK that received accelerated approval by the US FDA in August 2019 for the treatment of adults with *ROS1*-positive, metastatic NSCLC, and ≥12-year-old patients with solid tumors harboring an *NTRK* gene fusion.[14,15] In an integrated analysis of 3 phase I/II trials, entrectinib yielded strong and durable responses in patients with *ROS1* fusion-positive NSCLC and *NTRK* fusion-positive solid tumors.[16,17] Importantly, entrectinib treatment was associated with clinically meaningful intracranial responses, with an intracranial objective response rate of 55% in both patient groups.

While the mechanism of action of entrectinib on TRK and ROS1 is known, conflicting early information was reported on the distribution of this compound to the brain and its interaction with P-gp.[18] For example, initial data using classical bidirectional efflux ratio (ER) assays suggested that entrectinib and other molecules in its class (crizotinib and larotrectinib) are all strong substrates for P-gp, predicting poor brain penetration (see below). However, although entrectinib displayed low brain and cerebrospinal fluid (CSF) exposure in rats after a single oral dose, it achieved high brain-to-plasma concentration ratios (0.6–1.5) following repeated high daily doses in rat toxicology studies.[19] Therefore, clear evidence is needed to demonstrate that entrectinib can achieve clinically meaningful CNS exposures, associated with pharmacological activity and efficacy in CNS models, in order to support the scientific rationale for entrectinib as a treatment for brain tumors harboring *ROS1* and *NTRK* rearrangements.

In this study, we defined a novel ER calculation, apical efflux ratio (AP-ER), with the aim of obtaining a model that correlated better with in vivo brain distribution properties. We consider the AP-ER as a more physiologically relevant assessment, since it principally accounts for the polarized localization of P-gp (apical membrane). Using this new model, we characterized the interaction between entrectinib and P-gp in vitro and investigated the brain penetration, pharmacodynamic (PD) properties (via pathway biomarker signals), and antitumor activity of entrectinib in preclinical CNS models of cancer. The ability of entrectinib to penetrate the brain and its interaction with P-gp were compared with TKIs of a similar class, crizotinib (first-generation TKI for the treatment of *ROS1* fusion-positive NSCLC) and larotrectinib (first-generation TKI for the treatment of *NTRK* fusion-positive solid tumors).

Materials and Methods

Determination of P-gp Efflux Ratio by In Vitro Transcellular Studies

The substrate evaluations for P-gp presented in this article were all obtained from experiments performed

at F. Hoffmann-La Roche Ltd (Basel, Switzerland). Bidirectional permeability and P-gp efflux were measured using porcine kidney epithelial cells (LLC-PK1; used under a license agreement from the Schinkel group [The Netherlands Cancer Institute, Amsterdam]) stably transfected with human or murine P-gp (multidrug resistance protein 1, ATP binding cassette subfamily B member 1), as previously described.[20] These cell lines were cultured using standardized procedures (including mycoplasma testing), and each batch of cells was used within a 20-passage limit before resuscitation of new vials. The apparent permeability (P_{app}) related to transcellular transport, bidirectional ER, AP-ER, and mean bidirectional passive permeability in the presence of a P-gp inhibitor ($P_{app,inh}$) were calculated for entrectinib, crizotinib, larotrectinib, and digoxin (an in vitro benchmark P-gp substrate used as a control).

Briefly, on day 5 after plating, cell monolayers were evaluated for drug permeability in the apical-to-basolateral (A→B) and basolateral-to-apical (B→A) directions using a liquid handling robot (Tecan Group). Unless otherwise stated, test compounds were dosed at 1 µM. Samples were collected from triplicate wells of donor and receiver compartments after a 3.5-hour incubation in the presence or absence of a P-gp inhibitor (zosuquidar, 1 µM). Drug concentrations were measured by high-performance liquid chromatography–tandem mass spectrometry (LC-MS/MS).

P_{app} related to transcellular transport was calculated as follows:

$$P_{app} = \frac{\Delta Q}{\Delta t} \cdot \frac{1}{C_0 S} \quad (1)$$

where $\Delta Q/\Delta t$, C_0, and S represent the amount transported per time period, the initial concentration, and the transwell insert surface area, respectively.

The bidirectional (classic) ER was calculated as follows (see Fig. 1):

$$ER = \frac{P_{app}^{B\to A}}{P_{app}^{A\to B}} \quad (2)$$

where P_{app} is the apparent permeability in the basolateral-to-apical (B→A) direction and in the apical-to-basolateral (A→B) direction.

The newly designed AP-ER was calculated based on the permeability rates in the presence of a P-gp inhibitor $P_{app,inh}^{B\to A}$ or without a P-gp inhibitor $P_{app}^{B\to A}$ at the apical site: when a P-gp inhibitor was introduced, $P_{app,inh}^{B\to A}$ was considered equivalent to $P_{app,inh}^{A\to B}$

$$\text{AP-ER} = \frac{P_{app,inh}^{A\to B}}{P_{app}^{A\to B}} \quad (3)$$

Determination of Nonspecific Brain Tissue Binding In Vitro by Kinetic LIMBA

The kinetic lipid membrane binding assay (LIMBA) used in this study was based on the LIMBA screen assay as described by Assmus et al[21] and Belli et al.[22] The original setup was modified with the aims of reaching equilibrium faster by continuous stirring (particularly since entrectinib takes a long time to reach equilibrium), observing the kinetic properties of each drug, and calculating their half-lives to reach equilibrium and $logD_{BPL}$ (drug distribution coefficient between the aqueous phase and the porcine brain polar lipids extract) from the available ultraviolet (UV) data and a first-order kinetic model.

Briefly, a polyvinylidene fluoride filter disc coated with porcine brain polar lipids extract was inserted in a glass vial containing a 10 µM compound solution. The UV spectra of the compound in buffer, corresponding to the sample

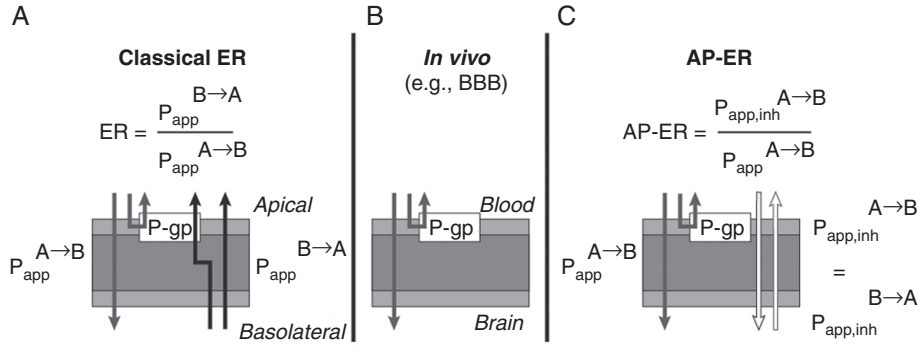

Fig. 1 In vitro P-gp transport assay: classic ER calculation versus the novel AP-ER approach. (A) The classic ER model is bidirectional and calculated as described. (B) In vivo, compounds reach the brain from the blood via the apical side only (unidirectional flow). (C) The novel AP-ER is calculated based on the permeability rates in the presence of a P-gp inhibitor or without a P-gp inhibitor at the apical site: when a P-gp inhibitor is introduced, the permeability rates in both directions are considered equivalent, mimicking in vitro conditions. AP-ER, apical efflux ratio; BBB, blood–brain barrier; ER, efflux ratio; P_{app}, apparent permeability in the basolateral-to-apical (B→A) direction and in the apical-to-basolateral (A→B) direction; $P_{app,inh}$, apparent permeability in the presence of an inhibitor; P-gp, P-glycoprotein.

concentration in the aqueous phase, were measured under controlled conditions (eg, continuous stirring to help reach the equilibrium much faster compared with the standard LIMBA) every 30 seconds. After the equilibrium was reached, the half-life ($t_{½}$; minutes) and $logD_{BPL}$ were derived from UV data and a first-order kinetic model. Unbound fraction (F_u) values in the brain were calculated as follows: $F_{u,brain} = \frac{1}{1+10^{\log D_{BPL}}}$.

A more detailed description of methods can be found in the Supplementary Materials section and Supplementary Figure 1.

Determination of Entrectinib Binding to Plasma Proteins from Rat, Mouse, and Human

Plasma protein binding was determined using equilibrium dialysis as described by Banker et al[23] and Zamek-Gliszczynski et al.[24] Briefly, dialysis sides of the 96-well high-throughput dialysis block (HTDialysis) were loaded with 0.15 mL of Søerensen phosphate buffer (pH 7.5). An equal volume of plasma spiked with the test compound was added to the sample side of each well, and the dialysis unit was sealed with a semipermeable adhesive cover and incubated at 37°C (5% CO_2) for 5 hours. At the end of dialysis, plasma and buffer samples were retrieved and drug concentrations quantified using LC-MS/MS. F_u values were calculated as a ratio of concentration in buffer after analysis to concentration in plasma after dialysis.

Animal Experiments

All animal studies were performed in adherence to the National Research Council Guidelines for the Care and Use of Laboratory Animals. The experimental preclinical testing protocols were approved by the Institutional Animal Care and Use Committee of the Cantonal Veterinary Office Basel, Switzerland. The animal facility was accredited by the Association for Assessment and Accreditation of Laboratory Animal Care.

Brain Distribution Study Following Intravenous Infusion in Rats

Male Sprague Dawley rats (n = 4 per time point) received a single i.v. bolus dose followed by i.v. infusion of the drug dissolved in vehicle (10 mM lactic acid and 5% glucose at pH 5.0). Animals were sacrificed 4–6 hours after the start of the infusion, and CSF, plasma, and brain samples were collected. The maximum feasible infusion time was 6 hours because entrectinib is a poorly soluble compound at the desired dose and needs to be dissolved in a vehicle with limited long-term tolerability. A detailed description of experimental design and collection schedule for plasma, CSF, and brain samples can be found in the Supplementary Materials and Supplementary Table 1.

Quantification of concentrations of entrectinib, crizotinib, and larotrectinib in plasma, brain, and CSF samples from rats

The drugs were extracted from 10 µL (entrectinib, crizotinib, and their internal standards) or 5 µL (larotrectinib and its internal standard) of either rat CSF/plasma, plasma, or brain homogenate samples by a protein precipitation procedure. Brain samples were homogenized with a 3-fold volume of blank rat plasma and quantified against a rat plasma calibration curve. For entrectinib and crizotinib, CSF samples were diluted with an equal volume of blank rat plasma immediately after collection and were quantified against a calibration curve in CSF/plasma (1:1). For larotrectinib, the CSF samples were diluted with an equal volume of bovine serum albumin immediately after collection. The samples were further diluted with blank rat plasma and quantified against a calibration curve in rat plasma.

All extracts were analyzed using reverse-phase liquid chromatography with gradient elusion. The compounds were detected and quantified by tandem mass spectrometry. Calibration curves were obtained by performing a linear regression (weighted 1/x2) on the calibration standards with lower limits of quantification (LLOQ) of 0.05 ng/mL for entrectinib and crizotinib CSF/plasma samples, 1.00 ng/mL for entrectinib and crizotinib plasma samples, and 0.25 ng/mL for larotrectinib CSF and plasma samples.

In Vivo PD, Efficacy, and Pharmacokinetics in KM12-Luc Intracranial Tumor Xenograft Mouse Model

PD and efficacy analyses

KM12 cells were labeled with a lentivirus expression vector under the promoter EF1a, and a stable pool (named hereafter as KM12-Luc) was generated after antibiotic selection. Thirty thousand KM12-Luc cells were then microinjected into the right lobe (*caudate nucleus*) of the brain of treatment-naïve female athymic nu/nu mice. Eleven (PD experiment) or 5 (efficacy experiment) days after cell inoculation, bioluminescence was measured by a Xenogen IVIS Lumina II Imaging System (Caliper Life Sciences). Mice were subsequently randomized based on bioluminescence intensity (BLI) and body weight. In the PD study, entrectinib was administered at 5, 15, 30, or 60 mg/kg twice daily (b.i.d.) for 3 doses. Terminal blood samples and intracranial (ITC) tumors were collected and snap-frozen 3, 8, and 12 hours after the last dose. Frozen tumors were lysed and quantitative western blotting was performed for phospho- and total phospholipase C gamma 1 (PLCγ1), AKT1, and S6 (see Supplementary Materials).

In the efficacy experiment, entrectinib was administered orally at a range of doses (1, 5, 15, 60 mg/kg b.i.d. or 10, 30 mg/kg once daily [q.d.]; n = 10/dose group) for 28 days. The bioluminescence signal and body weights were measured twice weekly. Plasma was collected from terminal bleeds and pharmacokinetic (PK) analyses were performed.

Quantification of entrectinib plasma concentrations in mice for PK analyses

Entrectinib and its stable isotopically labeled internal standard were extracted from 5 µL of mouse plasma by a protein precipitation procedure. The extracts were analyzed by LC-MS/MS using a gradient system. The compounds

were quantified by a triple quadrupole tandem mass spectrometer. Calibration curves were constructed by performing a linear regression (weighted 1/x2) of response ratios on the calibration standards with LLOQ of 1.0 ng/mL. Additional detailed methods for PK sampling and experiments are detailed in the Supplementary Materials section.

Statistical Analyses

For the statistical analyses, only group mean ± SD values were calculated for all in vitro and in vivo studies.

Results

Evaluation of In Vitro Efflux Assays for P-gp

The apparent permeability values and ERs of $P_{app}^{B\rightarrow A}$ to $P_{app}^{A\rightarrow B}$ for entrectinib, larotrectinib, crizotinib, and digoxin are listed in Table 1, as calculated based on the classical bidirectional in vitro assay using LLC-PK1 cell monolayers overexpressing human or mouse P-gp. All drugs displayed significantly high ERs (ER values ≥10) in both the classical human and mouse assays. However, based on the novel AP-ER model, larotrectinib and crizotinib yielded AP-ER values around or above those of the control digoxin, whereas entrectinib was associated with a noticeably lower AP-ER than the other drugs (Fig. 2, Table 1), which appears to be driven by a lack of effect of P-gp inhibition on the transport of entrectinib from apical side to basal side.

Unbound Fraction in Plasma Proteins and Rat Brain Tissue

The F_u values (mean ± SD) of entrectinib in human, mouse, and rat plasma samples were 0.0022 ± 0.0005, 0.0034 ± 0.0003, and 0.0032 ± 0.0009, respectively. No marked species difference in plasma protein binding was observed. The F_u values of crizotinib (0.057) and larotrectinib (0.349) in rat plasma were obtained from FDA pharmacology reviews of the drugs crizotinib and larotrectinib.[13,25]

The F_u in brain tissues and kinetic profiles of entrectinib, crizotinib, and larotrectinib estimated by the kinetic LIMBA are presented in Supplementary Table 2. Entrectinib demonstrated a longer half-life to reach equilibrium in the brain tissue ($t_{1/2}$ = 9.6 min) than the other 2 drugs (crizotinib: $t_{1/2}$ = 7.4 min; larotrectinib: $t_{1/2}$ = 6.2 min), suggesting that entrectinib takes a longer time to achieve equilibrium in the brain.

Brain Distribution Study Following Intravenous Infusion in Rats

The brain distribution study was conducted in rats following an i.v. bolus, then constant infusion of drug up to 6 hours. The mean concentrations measured in plasma, CSF, and brain for entrectinib, crizotinib, and larotrectinib are summarized in Table 2, along with the estimated

Table 1 In vitro P-gp activity of entrectinib, larotrectinib, and crizotinib in LLC-PK1 cells stably transfected with human or mouse P-gp

	In vitro P-gp activity (human)						In vitro P-gp activity (mouse)					
	ER	AP-ER	$P_{app}^{A\rightarrow B}$ nM/sec ± SD	$P_{app}^{B\rightarrow A}$ nM/sec ± SD	$P_{app,inh}^{A\rightarrow B}$ nM/sec ± SD	ER	AP-ER	$P_{app}^{A\rightarrow B}$ nM/sec ± SD	$P_{app}^{B\rightarrow A}$ nM/sec ± SD	$P_{app,inh}^{A\rightarrow B}$ nM/sec ± SD
Entrectinib	**15 [++]**	**1.1 [-]**	13.5 ± 3.4	197 ± 5	15.2 ± 1.9	**26 [++]**	**1.5 [-]**	9.90 ± 0.4	255 ± 19	14.6 ± 0.9
Larotrectinib	**10 [++]**	**2.8 [+]**	18.5	182 ± 37	51.9 ± 1.4	**20 [++]**	**6.3 [+]**	8.20 ± 0.7	161 ± 7	51.5 ± 2.1
Crizotinib	**28 [++]**	**3.5 [+]**	13.8 ± 0.3	388 ± 17	47.9 ± 10.5	**29 [++]**	**4.9 [+]**	12.0 ± 1.5	344 ± 16.8	58.6 ± 15.6
Digoxin[a]	**11 [++]**	**3.9 [+]**	10.9 ± 0.7	121 ± 7.3	42.0 ± 2.3	**10 [++]**	**3.4 [+]**	12.2 ± 1.0	125 ± 2.8	41.0 ± 3.8

[++] denotes very strong, [+] strong, or [-] weak substrate for P-gp. [a]Digoxin is an in vitro benchmark P-gp substrate, used as a control for the assay. ER was calculated from $P_{app}^{A\rightarrow B}$ and $P_{app}^{B\rightarrow A}$ (Equation 2); AP-ER was calculated from $P_{app}^{A\rightarrow B}$ and $P_{app,inh}^{A\rightarrow B}$ (Equation 3). A→B, apical-to-basolateral direction; AP-ER, apical efflux ratio; B→A, basolateral-to-apical direction; ER, efflux ratio; P_{app}, apparent permeability; $P_{app,inh}$, apparent permeability in the presence of a P-gp inhibitor (zosuquidar); P-gp, P-glycoprotein; SD, standard deviation.

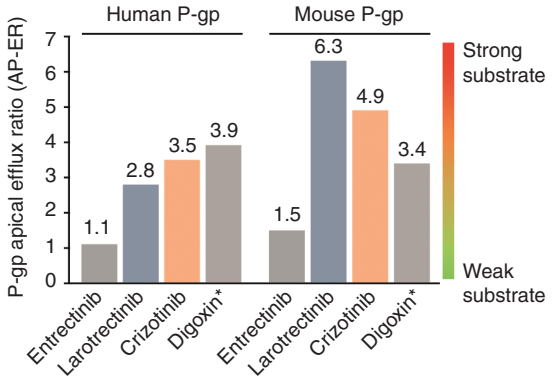

Fig. 2 In vitro P-gp AP-ER of entrectinib, larotrectinib, and crizotinib in LLC-PK1 cells stably transfected with human or mouse P-gp. Graphical representation of AP-ER (see Table 1) for entrectinib, larotrectinib, and crizotinib in human and mouse P-gp models. Based on this novel AP-ER model, entrectinib was shown to be a weak P-gp substrate, whereas larotrectinib and crizotinib were strong P-gp substrates. *Digoxin is an in vitro benchmark P-gp substrate, used as a control for the assay. AP-ER was calculated from $P_{app}^{A\rightarrow B}$ and $P_{app,inh}^{A\rightarrow B}$ (Equation 3). AP-ER, apical efflux ratio; P-gp, P-glycoprotein.

corresponding unbound concentration in plasma ($C_{u,p}$), unbound concentration in brain ($C_{u,b}$), and CSF/$C_{u,p}$ ratios.

At steady state (SS), there should be no difference (δ) in concentrations between 2 different time points. For entrectinib, δ in plasma was 140 nM; as this was within the SD values at each time point (109–430 nM), it was deemed to be close to SS. In brain, however, δ was large (276 nM) and greater than the SD (71.2–186), suggesting that SS in brain tissue had not been reached by 6 hours. This implies that the brain concentration of entrectinib measured at 6 hours may still be underestimated relative to SS. In contrast, for both crizotinib and larotrectinib, δ values in both plasma and brain were small and below or within their SDs, suggesting that SS was achieved.

Entrectinib presented the highest measured CSF/$C_{u,p}$ ratio at the measured time points: ~0.22 for entrectinib, compared with ~0.03 for crizotinib and larotrectinib, based on the average of 2 time points. All drugs in this rat infusion study achieved clinically relevant plasma exposure at efficacious dose (within 2-fold of the reported clinical concentrations): $C_{ave,ss}$ = 2000 nM (entrectinib), 874 nM (crizotinib), 423 nM (larotrectinib).[10,12,15]

In Vivo PD, Efficacy, and PK Study in KM12-Luc Intracranial Tumor Xenograft Mice

The PD effects on key signal pathway markers are presented in Supplementary Figure 2. In the KM12-Luc ITC mice, entrectinib treatment resulted in a potent and dose-dependent suppression of all key signaling nodes downstream of TRKA, including p-PLCγ1, pAKT, and pS6 with strong potency observed at doses ≥5 mg/kg b.i.d. Maximal inhibition was achieved at a dose level of 15 mg/kg b.i.d. and was well maintained with minimal reactivation through 8–12 hours.

Consistent with the brain penetration and expected antitumor activity of entrectinib, oral administration of 1 mg/kg b.i.d. of entrectinib resulted in a 35% inhibition of BLI relative to vehicle control at day 14, as shown in Fig. 3 and Supplementary Figure 3A. Tumor inhibition improved at 5 mg/kg b.i.d. and 10 mg/kg q.d., resulting in an 82.1% and 85.7% reduction, respectively, in BLI relative to control. Entrectinib demonstrated a strong antitumor activity at doses of 15 mg/kg b.i.d. (98.7% inhibition of BLI relative to control), 30 mg/kg q.d. (99.4% inhibition), and 60 mg/kg b.i.d. (100% inhibition). The reduction in tumor BLI signal was associated with improved survival of entrectinib-treated animals throughout the 28-day dosing window. Entrectinib was well tolerated at all dose levels tested (Supplementary Figure 3B). No vehicle-treated animals (0%; 0/9) survived through the dosing window, with all mice reaching terminal endpoints requiring euthanasia before day 21 (Fig. 3). At intermediate-to-low dose levels of entrectinib, there was improved survival; however, animals still succumbed to disease within the 28-day dosing window, with 0% (0/9) of mice at 1 mg/kg b.i.d., 11% (1/9) of mice at 5 mg/kg b.i.d., and 67% (6/9) mice at 10 mg/kg q.d. surviving through day 28. At higher doses of 15 mg/kg b.i.d., 30 mg/kg q.d., and 60 mg/kg b.i.d. of entrectinib, 100% of the mice survived throughout the dosing window.

The PK parameters of entrectinib across the range of doses studied are summarized in Table 3 and Supplementary Figure 4. To assess variability and dose-exposure relationship, the PK parameters (area under the curve [AUC], maximum concentration) from different dosing groups and dosing days were plotted. The exposure increased with increasing dose, and there was no apparent accumulation on day 2 or day 8 compared with day 1. Because the efficacy was independent of dosing schedule (ie, b.i.d. vs q.d.), the AUC was evaluated based on total daily dose. At a daily dose of 30 mg/kg—for which robust tumor inhibition, high survival rates, and maximum inhibition of TRK pathway biomarkers were observed—the AUC_{24h} ranged from 24.5 to 54.8 μM·h (mean of 38.3 μM·h), resulting in an average plasma concentration of ~1.6 μM (AUC_{24h}/24 hours).

Discussion

Entrectinib was specifically selected during the discovery stage because it has the potential to achieve high brain-to-plasma concentration ratios.[18] However, in a single oral-dose, in vivo PK study of rats treated with 20 mg/kg entrectinib, the concentrations of this compound in the CSF were inferior to the LLOQ (1 nM), with a brain-to-plasma concentration ratio of 0.185 (data not shown). As the free plasma concentration $C_{u,p}$ at this time point was around 5 nM, the results of this in vivo study seemed inconsistent with the expectation of a high brain penetration property. Contrary to what was observed in the single-dose studies, entrectinib distributed well into the brain in several in vivo repeated-dose studies: the brain-to-plasma concentration ratios of entrectinib were higher, at ~0.4 in

Table 2 Mean concentrations ($n = 4$) of entrectinib, crizotinib and larotrectinib in plasma, CSF and brain from rats after single i.v. bolus followed by i.v. infusion

Parameters	Entrectinib		Crizotinib		Larotrectinib	
	5 h	6 h	5 h	6 h	4 h	5 h
Plasma concentration, nM ± SD	1260 ± 430	1400 ± 109	477 ± 53.7	489 ± 47.9	330 ± 46.3	332 ± 82.2
δ plasma concentration at SS, nM (SD)	140 (109–430)		12 (47.9–53.7)		2 (46.3–82.2)	
Brain concentration, nM ± SD	567 ± 71.2	843 ± 186	390 ± 12.1	477 ± 131	21.4 ± 3.74	23.0 ± 5.60
δ brain concentration at SS, nM (SD)	276 (71.2–186)		87 (12.1–131)		1.6 (3.74–5.60)	
CSF concentration, nM ± SD	0.99 ± 0.2	0.81 ± 0.2	1.1 ± 0.36	0.78 ± 0.18	3.16 ± 0.76	3.56 ± 0.87
Unbound plasma concentration ($C_{u,p}$), nM[a]	4.0	4.5	27	28	115	116
Unbound brain concentration ($C_{u,b}$), nM[b]	0.28	0.42	0.94	1.1	9.9	11
Measured CSF/$C_{u,p}$ ratio	0.25	0.18[c]	0.041	0.028[d]	0.027	0.031[e]

[a]$C_{u,p}$ value initially calculated as product of mean plasma concentration by plasma F_u, and later determined using equilibrium dialysis in vitro.
[b]$C_{u,b}$ value was initially calculated as the product of mean brain concentration by brain F_u, and later determined using kinetic LIMBA.
[c]SS not reached after 6 hours.
[d]Near SS after 6 hours.
[e]Near SS after 5 hours.
δ, difference in concentrations between two different time points; CSF, cerebrospinal fluid; $C_{u,b}$, unbound drug concentration in brain; $C_{u,p}$, unbound drug concentration in plasma; F_u, unbound fraction; i.v., intravenous; LIMBA, lipid membrane binding assay; SD, standard deviation; SS, steady state.

mice, 0.6–1.5 in rats, and 1.4–2.2 in dogs at 24 hours post last dose following repeated oral daily dosing of the compound.[19] A possible explanation for this apparent discrepancy is that entrectinib takes a long time to reach SS and was, therefore, not apparent following single doses. In our brain infusion experiment, entrectinib had not reached SS by 6 hours (6 hours is the maximum feasible time for infusions using this vehicle, see Methods) while in the kinetic LIMBA with brain tissue, entrectinib had a longer $t_{1/2}$ of 9.6 minutes to reach equilibrium compared with other kinase inhibitors tested in the present work.

Because total brain-to-plasma concentration ratios are not sufficient to support good brain penetration of basic compounds in particular, P-gp ERs were measured for entrectinib, crizotinib, and larotrectinib. The high ER observed for the 3 drugs using a classic P-gp model suggested that they are all strong P-gp substrates and should be unlikely to have sustained exposure in the brain based on previous modeling.[20] Due to the discrepancy between in vivo data and the classic bidirectional permeability model, we designed an alternative, unidirectional P_{app} model.

This model used the AP-ER to assess P-gp substrate interaction for entrectinib, crizotinib, larotrectinib, and digoxin using P-gp–expressing LLC-PK1 cell lines. In this model, AP-ER was defined as the ratio of $P_{app,inh}^{A\rightarrow B}$ in the presence of a P-gp inhibitor versus $P_{app}^{A\rightarrow B}$ in the absence of a P-gp inhibitor. In vivo, compounds reach the brain from the blood via the apical side only; hence, the AP-ER was used to more closely mimic in vivo conditions, since P-gp is located on the apical side only. Interestingly, our in vitro data showed that entrectinib $P_{app}^{A\rightarrow B}$ was not sensitive to P-gp activity, with similar values observed in the presence or absence of a P-gp inhibitor. Moreover, entrectinib demonstrated a distinctively lower AP-ER compared with crizotinib, larotrectinib, and digoxin, indicating a weaker interaction of entrectinib with P-gp. As AP-ER for entrectinib was <2 for both the mouse and human P-gp assays, we concluded that entrectinib is a weak P-gp substrate. The discrepancy between the classical ER and AP-ER for entrectinib is likely related to its "atypical" physicochemical properties, including a very high lipophilicity/amphiphilicity that leads to strong membrane partitioning and a lower than normal recovery from the assay. These properties may contribute to an asymmetric interaction with the cell membrane and P-gp, depending on whether the compound is dosed from the apical-to-basolateral (A→B) or basolateral-to-apical (B→A) direction.

The AP-ER approach is not only superior for the assessment of brain penetration, it is also less experimentally demanding without compromising discriminatory power, when applied as a broad screening model for P-gp substrate testing, as demonstrated recently by Ohashi et al.[26] In their study, Ohashi et al developed a nearly identical approach to ours, using an inhibitor of P-gp (cyclosporin A) to calculate a unidirectional flux ratio (UFR), a measure that is essentially equivalent to the AP-ER we used. In their UFR model, compounds with a UFR (AP-ER) <2.6 were considered non-substrates or weak substrates of P-gp, which is consistent with our findings and interpretation that entrectinib (AP-ER <2) interacts weakly with the P-gp transporter.

Importantly, the differences observed between the 3 TKIs based on the novel AP-ER model were confirmed in the in vivo brain distribution study following i.v. infusion of these compounds. Indeed, entrectinib showed a more favorable CSF/$C_{u,p}$ ratio (>0.2) than crizotinib and larotrectinib (both ~0.03) under SS conditions. These in vivo CSF/$C_{u,p}$ ratios are mostly consistent with the low AP-ER observed for entrectinib (1.1–1.5) compared with the high AP-ER measured for crizotinib and larotrectinib (both ≥2.8). Of note, the CSF/$C_{u,p}$ ratio for entrectinib may still be underestimated

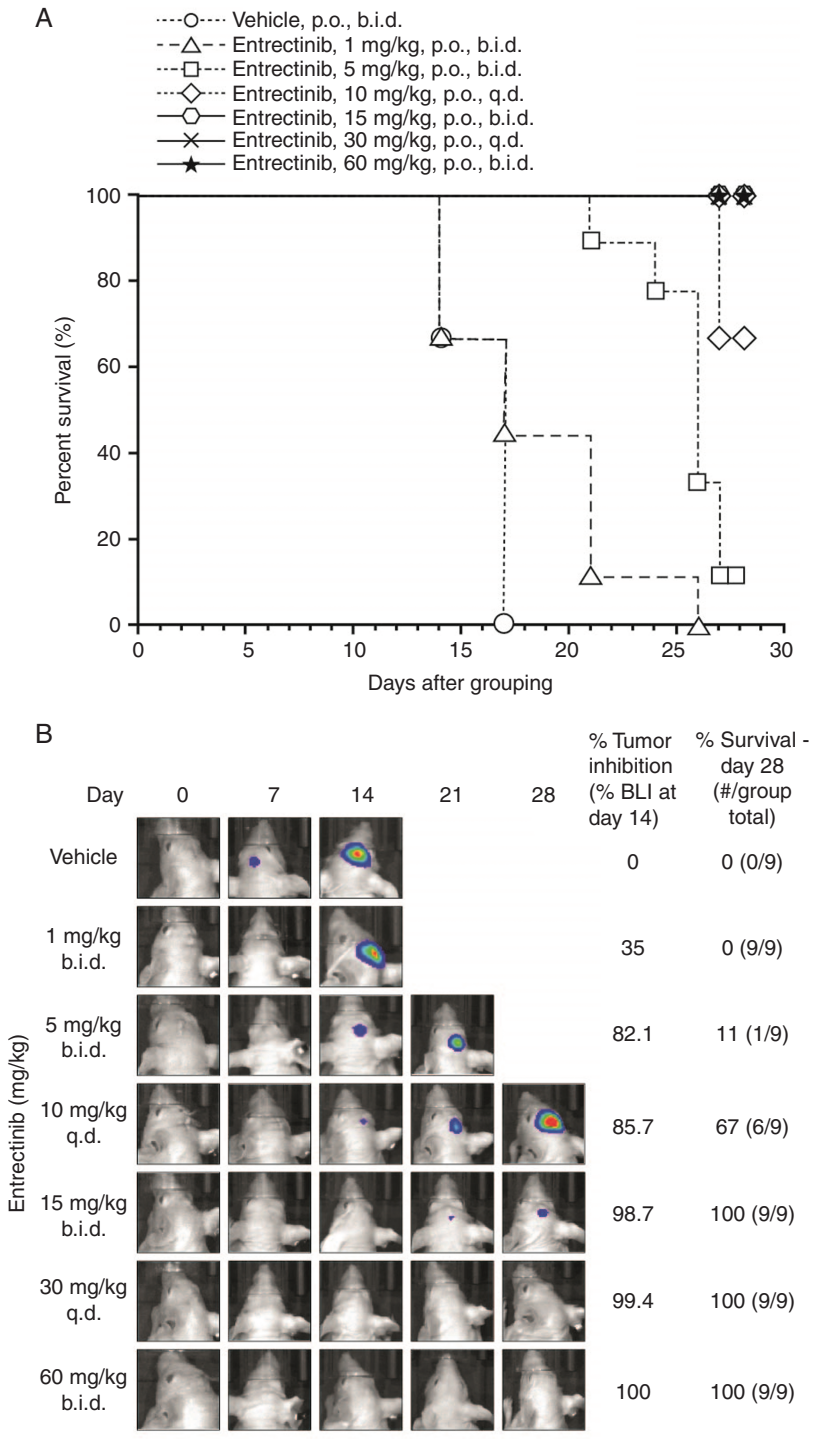

Fig. 3 Antitumor efficacy of entrectinib in the ITC-inoculated KM12-Luc tumor model. Thirty thousand KM12-Luc cells were micro-injected into the right lobe of the brain of treatment-naïve female athymic nu/nu mice. Entrectinib was administered orally for 28 days at a range of doses. (A) Percentage of animals alive over time after treatment with vehicle or entrectinib at doses of 1, 5, 15, 60 mg/kg b.i.d. or 10 or 30 mg/kg q.d. (B) Bioluminescence signal observed in animals treated with vehicle or entrectinib at doses of 1, 5, 15, 60 mg/kg b.i.d., or 10, 30 mg/kg q.d. for 28 days. All vehicle-treated animals died by day 17. b.i.d., twice daily; BLI, bioluminescence inhibition; ITC, intracranial; p.o., orally; q.d., once daily.

because SS in brain was not achieved; nevertheless, it was ~7-fold higher than the ratio for crizotinib and larotrectinib. Moreover, the estimated $C_{u,b}$ based on the total concentration in whole brain homogenate and the F_u estimated by the novel kinetic LIMBA were remarkably similar to directly measured CSF concentrations (≤3-fold

Table 3 Mean AUC_{24h} of entrectinib in plasma after oral administration to KM12-Luc ITC tumor-bearing Balb/c nude mice

Total daily dose (mg/kg/day)	Mean AUC_{24h} (μM·h)	n[a]	Range (μM·h)
2 (1 mg/kg b.i.d.)	1.3	2	1.06–1.50
10 (5 mg/kg b.i.d. and 10 mg/kg q.d.)	11.3	5	6.3–18.3
30 (15 mg/kg b.i.d. and 30 mg/kg q.d.)	38.3	5	24.5–54.8
60 (30 mg/kg b.i.d.)	45.3	1	45.3
120 (60 mg/kg b.i.d.)	99.9	3	90.1–113.0

[a]Number of treatment groups across experiments and evaluation days; each group had 3 or 4 animals per time point.
AUC_{24h}, area under the curve over 24 hours; b.i.d., twice daily; ITC, intracranial; q.d., once daily.

variation), considering the variables affecting the different assays. This consistency supports the use of CSF concentrations as a reasonable surrogate of active exposures in the brain for the molecules tested in this study.

Although entrectinib is described as a weak P-gp substrate in this report based on preclinical studies, it is highly likely not a human P-gp substrate at all, in line with what was described by the US prescribing information.[15] This prediction is based on the AP-ER of 1.1 (human P-gp assay), a good oral bioavailability in humans (>50%, data on file), and the limited effects of co-administrating intraconazole, an inhibitor of CYP3A and P-gp, on entrectinib absorption after a single oral dose of entrectinib at 100 mg in patients.[15]

Consistent with its good brain distribution and weak P-gp interaction, entrectinib demonstrated strong PD effects associated with TRK pathway biomarkers, namely, p-PLCγ1, pAKT, and pS6, in brain tumor tissues, and robust efficacy as determined by tumor growth inhibition and survival rates in an intracranial KM12-Luc colorectal tumor (expressing *TPM3-NTRK1*) mouse model. These results are in line with previous reports that entrectinib demonstrated tumor growth inhibition and full survival benefit in an intracranial *NTRK1* fusion-positive model of primary CNS tumor (BNN2 and BNN4; gliomas) at clinically relevant systemic exposures.[27] Importantly, following daily oral administration of entrectinib for 28 days in the intracranial KM12-Luc tumor model, a similar efficacy was achieved when animals were given the same total daily dose regardless of dosing frequency, suggesting that antitumor activity is dependent on only total daily exposure, rather than on peak or trough concentrations of entrectinib.

The plasma concentration of entrectinib, which is the major circulating drug-related component in rodent species (data not shown), was measured at multiple time points to determine PK parameters in both the efficacy and PD studies in mice bearing intracranial KM12-Luc tumors. As a very limited volume of blood could be collected from each mouse, a sparse sampling approach was used. Only one AUC value could be obtained in each treatment group on each sampling day, and the AUC was evaluated based on a total daily dose, as efficacy was independent of dosing schedule. Interestingly, at the recommended human oral dose of 600 mg/kg q.d., the observed AUC_{24h} of entrectinib at SS in patients was reported to be 48 μM·h with an estimated average plasma concentration of approximately 2.0 μM,[15] which encompasses the level of exposure needed to observe a response in the intracranial KM12-Luc tumor xenograft mouse model. This is 43% higher than what was achieved (1.4 μM) after a 6-hour infusion of entrectinib in rats.

Based on the conservative assumption of a similar $CSF/C_{u,p}$ ratio for rat and human, the CSF concentration of entrectinib in patients should be >0.9 nM following repeated oral dose of 600 mg entrectinib. Furthermore, the predicted CSF concentration of entrectinib is ~4 nM at SS in humans (Fischer et al, in preparation), taking into account the human plasma F_u of 0.0022 and the human AP-ER of 1.1, based on a new in-house model developed by using a large number of molecules with measured AP-ER and in vivo brain distribution values. The CSF value of entrectinib is approximately greater than or equal to the half-maximal inhibitory concentration (IC_{50}) of entrectinib for TRKA/B/C and ROS1 (0.1–1.7 nM; Supplementary Materials and Supplementary Table 3). For comparison, the expected CSF levels for crizotinib and larotrectinib in patients are lower than the targeted IC_{50}; the IC_{50} of crizotinib against ROS1 kinase was 40–60 nM,[28] while the IC_{50} of larotrectinib against TRKA/B/C was 5–11 nM.[6] Importantly, larotrectinib is also a substrate of breast cancer resistance protein (BCRP; another known efflux transporter of the blood–brain barrier), whereas entrectinib and crizotinib are not.[10,15,29] BCRP (along with P-gp) may, therefore, also be contributing to the poor brain penetration of larotrectinib.

In conclusion, entrectinib is an effective brain penetrant and a weak P-gp substrate, contrary to crizotinib and larotrectinib, which achieved limited brain penetration and were strong P-gp substrates. Furthermore, entrectinib showed strong CNS efficacy in our brain tumor model, consistent with the clinical efficacy observed in patients with *NTRK* fusion-positive solid tumors or *ROS1* fusion-positive NSCLC who presented with brain metastases or primary CNS tumors.[16,17]

Overall, entrectinib is different from other currently available TKIs of the same class, because it is expected to enable selective targeting of brain tumors (either primary or metastatic) harboring *NTRK* or *ROS1* gene fusions. Our findings also have broad implications for the preclinical characterization of new molecular entities for treating CNS cancers.

Supplementary Material

Supplementary data are available at *Neuro-Oncology* online.

Keywords

CNS-active | entrectinib | P-gp | ROS1 |TRK

Funding

This study was supported by F. Hoffmann-La Roche Ltd/ Genentech Inc. All authors are or were employees of Roche/ Genentech at the time of the study.

Acknowledgments

The authors would like to thank Georgina Meneses-Lorente, Pawel Dzygiel, and Monique Wittig for their scientific review and technical assistance. We also acknowledge the valuable contribution of Carina Cantrill, Marie-Elise Brun, Marie-Stella Gruyer, Christelle Rapp, Véronique Dall'Asen, Thomas Thelly, Sara Belli, Neil Parrott, Jochem Alsenz, Luca Ferrari, and Gaurav Tyagi. Third-party medical writing assistance, under the direction of the authors, was provided by Laura Vergoz, PhD, of Gardiner-Caldwell Communications, and was funded by F. Hoffmann-La Roche Ltd. Part of these data were previously presented at the AAPS PharmSci 360 conference (November 3–6, 2019).

Conflict of interest statement. All authors are or were employees of Roche/Genentech. F.V. is currently an employee of Merck & Co. Inc., and L.Y. is currently working at LIYU Pharmaceutical Consulting LLC, but both were employees of Roche at the time of study conduct.

References

1. Stransky N, Cerami E, Schalm S, Kim JL, Lengauer C. The landscape of kinase fusions in cancer. *Nat Commun.* 2014;5:4846.
2. Kotecha R, Gondi V, Ahluwalia MS, Brastianos PK, Mehta MP. Recent advances in managing brain metastasis. *F1000Res.* 2018;7:1772.
3. Arrieta O, Villarreal-Garza C, Zamora J, et al. Long-term survival in patients with non-small cell lung cancer and synchronous brain metastasis treated with whole-brain radiotherapy and thoracic chemoradiation. *Radiat Oncol.* 2011;6:166.
4. Heffron TP. Challenges of developing small-molecule kinase inhibitors for brain tumors and the need for emphasis on free drug levels. *Neuro Oncol.* 2018;20(3):307–312.
5. Neul C, Schaeffeler E, Sparreboom A, Laufer S, Schwab M, Nies AT. Impact of membrane drug transporters on resistance to small-molecule tyrosine kinase inhibitors. *Trends Pharmacol Sci.* 2016;37(11):904–932.
6. Drilon A, Laetsch TW, Kummar S, et al. Efficacy of larotrectinib in TRK fusion-positive cancers in adults and children. *N Engl J Med.* 2018;378(8):731–739.
7. Costa DB, Kobayashi S, Pandya SS, et al. CSF concentration of the anaplastic lymphoma kinase inhibitor crizotinib. *J Clin Oncol.* 2011;29(15):e443–e445.
8. Dagogo-Jack I, Shaw AT. Crizotinib resistance: implications for therapeutic strategies. *Ann Oncol.* 2016;27(Suppl 3):iii42–iii50.
9. Shaw AT, Riely GJ, Bang YJ, et al. Crizotinib in ROS1-rearranged advanced non-small-cell lung cancer (NSCLC): updated results, including overall survival, from PROFILE 1001. *Ann Oncol.* 2019;30(7):1121–1126.
10. US FDA. *VITRAKVI prescribing information.* 2019. http://labeling.bayerhealthcare.com/html/products/pi/vitrakvi_PI.pdf. Accessed January 28, 2020.
11. Rosen EY, Schram AM, Young RJ, et al. Larotrectinib demonstrates CNS efficacy in TRK fusion-positive solid tumors. *J Clin Oncol Precis Oncol.* 2019;3:1–5.
12. US FDA. *XALKORI prescribing information.* 2017. https://www.accessdata.fda.gov/drugsatfda_docs/label/2017/202570s021lbl.pdf. Accessed January 28, 2020.
13. US FDA CDER. *VITRAKVI multi-disciplinary review and evaluation.* 2018. https://www.accessdata.fda.gov/drugsatfda_docs/nda/2018/210861Orig1s000_211710Orig1s000MultidisciplineR.pdf. Accessed January 28, 2020.
14. Ardini E, Menichincheri M, Banfi P, et al. Entrectinib, a Pan-TRK, ROS1, and ALK inhibitor with activity in multiple molecularly defined cancer indications. *Mol Cancer Ther.* 2016;15(4):628–639.
15. US FDA. *ROZLYTREK prescribing information.* 2019. https://www.accessdata.fda.gov/drugsatfda_docs/label/2019/212725s000lbl.pdf. Accessed January 28, 2020.
16. Drilon A, Siena S, Dziadziuszko R, et al; trial investigators. Entrectinib in ROS1 fusion-positive non-small-cell lung cancer: integrated analysis of three phase 1-2 trials. *Lancet Oncol.* 2020;21(2):261–270.
17. Doebele RC, Drilon A, Paz-Ares L, et al; trial investigators. Entrectinib in patients with advanced or metastatic NTRK fusion-positive solid tumours: integrated analysis of three phase 1-2 trials. *Lancet Oncol.* 2020;21(2):271–282.
18. Menichincheri M, Ardini E, Magnaghi P, et al. Discovery of entrectinib: a new 3-aminoindazole as a potent anaplastic lymphoma kinase (ALK), c-ros oncogene 1 kinase (ROS1), and pan-tropomyosin receptor kinases (Pan-TRKs) inhibitor. *J Med Chem.* 2016;59(7):3392–3408.
19. de la Cruz CC, Hunsaker T, Vazvaei F, Draganov D, Yu L, Merchant M. Determination of the efficacious Entrectinib exposures required for pathway inhibition and anti-tumor activity in a subcutaneous and intracranial TPM3-NTRK1mutant tumor model. *Cancer Res* 2019;79:3894.
20. Poirier A, Cascais AC, Bader U, et al. Calibration of in vitro multidrug resistance protein 1 substrate and inhibition assays as a basis to support the prediction of clinically relevant interactions in vivo. *Drug Metab Dispos.* 2014;42(9):1411–1422.
21. Assmus F, Seelig A, Gobbi L, Borroni E, Glaentzlin P, Fischer H. Label-free assay for the assessment of nonspecific binding of positron emission tomography tracer candidates. *Eur J Pharm Sci.* 2015;79:27–35.
22. Belli S, Assmus F, Wagner B, et al. Estimation of drug binding to brain tissue: methodology and in vivo application of a distribution assay in brain polar lipids. *Mol Pharm.* 2015;12(12):4529–4541.
23. Banker MJ, Clark TH, Williams JA. Development and validation of a 96-well equilibrium dialysis apparatus for measuring plasma protein binding. *J Pharm Sci.* 2003;92(5):967–974.
24. Zamek-Gliszczynski MJ, Ruterbories KJ, Ajamie RT, et al. Validation of 96-well equilibrium dialysis with non-radiolabeled drug for definitive measurement of protein binding and application to clinical development of highly-bound drugs. *J Pharm Sci.* 2011;100(6):2498–2507.
25. US FDA CDER. *XALKORI pharmacology review(s).* 2011. https://www.accessdata.fda.gov/drugsatfda_docs/nda/2011/202570Orig1s000PharmR.pdf. Accessed January 28, 2020.

26. Ohashi R, Watanabe R, Esaki T, et al. Development of simplified in vitro P-glycoprotein substrate assay and in silico prediction models to evaluate transport potential of P-glycoprotein. *Mol Pharm.* 2019;16(5):1851–1863.

27. Cook PJ, Thomas R, Kannan R, et al. Somatic chromosomal engineering identifies BCAN-NTRK1 as a potent glioma driver and therapeutic target. *Nat Commun.* 2017;8:15987.

28. Shaw AT, Ou SH, Bang YJ, et al. Crizotinib in ROS1-rearranged non-small-cell lung cancer. *N Engl J Med.* 2014;371(21):1963–1971.

29. US FDA CDER. *XALKORI clinical pharmacology and biopharmaceutics review(s).* 2011. https://www.accessdata.fda.gov/drugsatfda_docs/nda/2011/202570Orig1s000ClinPharmR.pdf. Accessed January 28, 2020.